Letter

## Profiling spin and orbital texture of a topological insulator in full momentum space

H. Bentmann , <sup>1,\*</sup> H. Maaß, <sup>1</sup> J. Braun, <sup>2</sup> C. Seibel, <sup>1</sup> K. A. Kokh, <sup>3,4,5</sup> O. E. Tereshchenko, <sup>3,6</sup> S. Schreyeck, <sup>7</sup> K. Brunner, <sup>7</sup> L. W. Molenkamp, <sup>7</sup> K. Miyamoto, <sup>8</sup> M. Arita, <sup>8</sup> K. Shimada , <sup>8</sup> T. Okuda, <sup>8</sup> J. Kirschner, <sup>9</sup> C. Tusche, <sup>9,10,11</sup> H. Ebert, <sup>2</sup> J. Minár, <sup>12</sup> and F. Reinert <sup>1</sup>

\*\*Experimentelle Physik VII and Würzburg-Dresden Cluster of Excellence ct.qmat,

<sup>1</sup>Experimentelle Physik VII and Würzburg-Dresden Cluster of Excellence ct.qmat,
Universität Würzburg, Am Hubland, D-97074 Würzburg, Germany, European Union

<sup>2</sup>Department Chemie, Physikalische Chemie, Universität München,
Butenandtstrasse 5-13, D-81377 München, Germany, European Union

<sup>3</sup>Novosibirsk State University, 636090 Novosibirsk, Russia

<sup>4</sup>Institute of Geology and Mineralogy, SB RAS, 630090 Novosibirsk, Russia

<sup>5</sup>Kemerovo State University, 650000 Kemerovo, Russia

<sup>6</sup>Institute of Semiconductor Physics, 636090 Novosibirsk, Russia

<sup>7</sup>Institute for Topological Insulators and Physikalisches Institut, Experimentelle Physik III,
Universität Würzburg, Am Hubland, D-97074 Würzburg, Germany, European Union

<sup>8</sup>Hiroshima Synchrotron Radiation Center, Hiroshima University, Kagamiyama 2-313, Higashi-Hiroshima 739-0046, Japan

<sup>9</sup>Max-Planck-Institut für Mikrostrukturphysik, Weinberg 2, D-06120 Halle, Germany, European Union

<sup>10</sup>Forschungszentrum Jülich, Peter Grünberg Institut (PGI-6), D-52425 Jülich, Germany, European Union

<sup>11</sup>Fakultät für Physik, Universität Duisburg-Essen, D-47057 Duisburg, Germany, European Union

<sup>12</sup>New Technologies-Research Center, University of West Bohemia, Univerzitni 8, 306 14 Pilsen, Czech Republic, European Union



(Received 19 November 2020; accepted 1 April 2021; published 15 April 2021)

We investigate the coupled spin and orbital textures of the topological surface state in  $Bi_2(Te,Se)_3(0001)$  across full momentum space using spin- and angle-resolved photoelectron spectroscopy and relativistic one-step photoemission theory. For an approximately isotropic Fermi surface in  $Bi_2Te_2Se$ , the measured intensity and spin momentum distributions, obtained with linearly polarized light, qualitatively reflect the orbital composition and the orbital-projected in-plane spin polarization, respectively. In  $Bi_2Te_3$ , the in-plane lattice potential induces a hexagonal anisotropy of the Fermi surface, which manifests in an out-of-plane photoelectron spin polarization with a strong dependence on light polarization, excitation energy, and crystallographic direction.

DOI: 10.1103/PhysRevB.103.L161107

Topological states of matter are playing a central role in modern condensed-matter physics. Initiated by the discovery of topological insulators [1,2], a variety of topological material classes has been established over the past decade, including topological crystalline insulators [3], quantum-anomalous-Hall systems [4], Weyl semimetals [5], and, more recently, intrinsic magnetic topological insulators [6]. In these systems, spin-orbit interaction induces a spin polarization in the electronic structure and is essential for generating the topologically nontrivial properties. In the case of topological insulators, in particular, spin-orbit coupling allows for the presence of a single spin-polarized topological surface state (TSS) and gives rise to the characteristic spin-momentum locking on the Fermi surface of the TSS [2].

The spin-momentum locking of the TSS is eventually rooted in the microscopic spin and orbital degrees of freedom and manifests in characteristic spin and orbital textures in momentum space [7,8]. Angle-resolved photoelectron spectroscopy (ARPES) combined with spin detection and photoexcitation by light of varying polarization has been a powerful approach to directly address these momen-

tum textures in topological insulators experimentally [8–19]. However, while the momentum-resolved photoelectron intensity is routinely measured, probing the photoelectron spin polarization over wide regions in momentum space poses a challenge and has become possible only recently [20–22]. This has typically restricted the bulk of previous results to selected points in momentum space. In the present work, we present spin-resolved ARPES experiments for the prototypical topological insulator Bi<sub>2</sub>(Te,Se)<sub>3</sub>(0001). We analyze the momentum distributions of photoelectron spin polarization and photoelectron intensity on equal footing and in dependence of light polarization. Supported by relativistic one-step photoemission calculations and model considerations, the experimental data unveil the full momentum dependence of the coupled spin and orbital textures of the TSS.

The spin-resolved ARPES experiments on Bi<sub>2</sub>Te<sub>2</sub>Se were performed using a momentum microscope with a two-dimensional (2D) imaging spin filter [21,23]. The fourth harmonic of a Ti:Sa oscillator served as the light source ( $h\nu = 6 \text{ eV}$ ). The measurement geometry is shown in Fig. 1(a), where  $\alpha = 8^{\circ}$ . The energy resolution in the spin-resolved momentum maps was set to 20 meV. The measurements were performed at T = 130 K and at pressures of the order of  $p = 10^{-10}$  mbar. The spin-resolved data were processed as described in [20,21]. Thin films of Bi<sub>2</sub>Te<sub>2</sub>Se were grown by

<sup>\*</sup>Corresponding author: hendrik.bentmann@physik.uni-wuerzburg.de

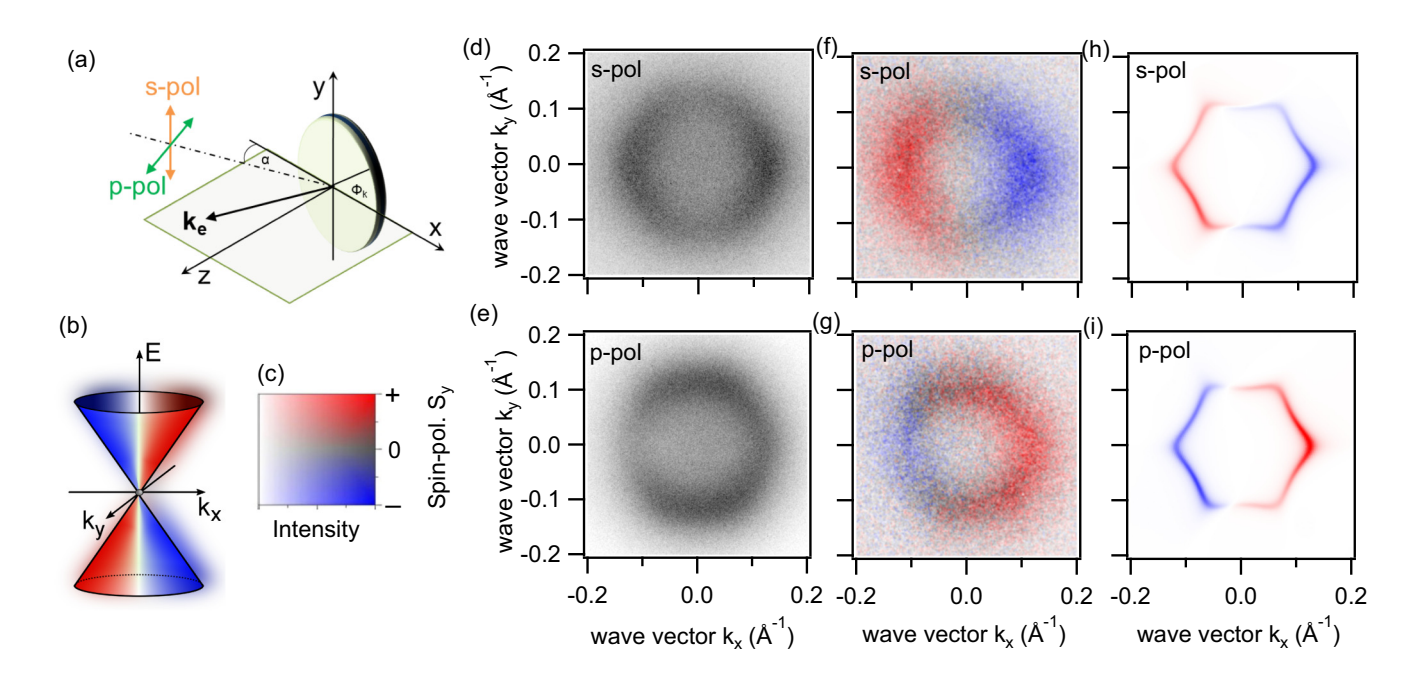


FIG. 1. (a) Sketch of the experimental geometry. (b) Schematic of a topological surface state with helical spin texture. (c) Color code for the measured spin-resolved momentum distributions in (f) and (g). Momentum distributions of the (d), (e) photoelectron intensity and (f), (g) photoelectron spin polarization measured with s- and p-polarized light ( $h\nu = 6 \text{ eV}$ ) for the topological surface state in Bi<sub>2</sub>Te<sub>2</sub>Se(0001). (h), (i) Relativistic one-step photoemission calculations corresponding to the experimental results in (f) and (g). The spin-quantization axis in experiment and theory is along y. All measurements were carried out at a temperature of ~130 K.

molecular beam epitaxy and prepared for measurement as described elsewhere [24,25]. The measurements on Bi<sub>2</sub>Te<sub>3</sub> were performed at the Hiroshima synchrotron radiation center (HiSOR). Spin-resolved data were collected at the efficient spin-resolved spectroscopy endstation (ESPRESSO) at BL-9B [26]. The spin detector is based on very low energy electron diffraction (VLEED) and projects the photoelectron spin to the variable axis of magnetization of the target surface [26,27]. Supplementary spin-integrated data were obtained at BL-9A. At both setups, the angle of incidence was  $\alpha = 40^{\circ}$ . The Bi<sub>2</sub>Te<sub>3</sub> single crystal, grown by a modified vertical Bridgman method [28], was cleaved along the (0001) direction under ultrahigh vacuum (UHV) conditions at room temperature. The experiments were carried out at pressures below  $4 \times 10^{-10}$  mbar and at  $T \approx 70$  K. A schematic of the experimental geometry is shown in Fig. 1(a).

For the electronic structure calculations from first principles, we used the SPR-KKR package based on the Korringa-Kohn-Rostoker method and the Dirac equation, to take into account all relativistic effects [29]. Our spectroscopical analysis is based on the fully relativistic one-step model in its spin-density-matrix formulation [30]. To take care of impurity scattering, a small constant imaginary value of  $V_{il} = 0.01 \text{ eV}$  was used for the initial state. For the final state, a constant imaginary value of  $V_{ih} = 2.0 \text{ eV}$  has been chosen. A more detailed description of the electronic structure calculations and of the spectroscopic analysis is given in the Supplemental Material [31], which includes Refs. [32–36].

Figure 1 provides an overview of our polarization-dependent ARPES measurements of the TSS in  $Bi_2Te_2Se(0001)$ . The intensity distributions in Figs. 1(d)

and 1(e) display characteristically different textures for *s*- and *p*-polarized light, in agreement with previous work [13,15]. A quantitative analysis of the intensities in Figs. 2(a) and 2(b) reveals an approximate  $\cos^2 \phi_k$  azimuthal dependence for *s* polarization, where  $\phi_k$  is the azimuthal angle along a constant

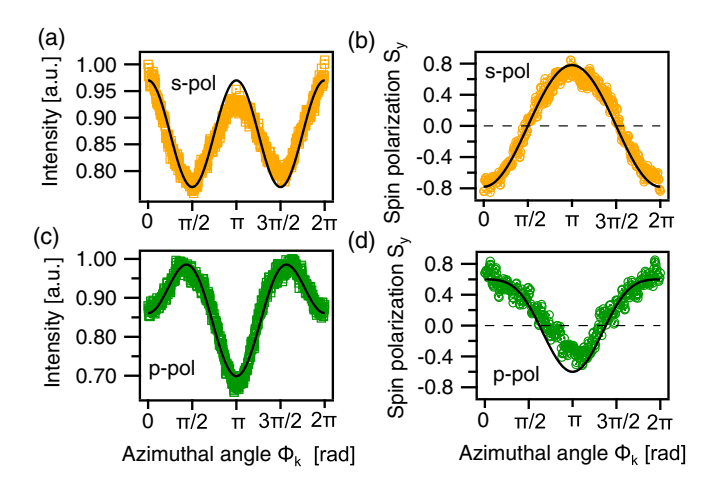


FIG. 2. Azimuthal-angle  $\phi_k$  dependence of the photoemission intensity/spin polarization measured in (a), (b) *s*-polarized geometry and (c), (d) *p*-polarized geometry.  $\phi_k$  is the azimuthal angle along a constant energy contour [cf. Figs. 1(d)–1(g)] and  $\phi_k = 0$  corresponds to the positive  $k_x$  axis. For a given  $\phi_k$ , the (a), (c) maximal intensity and (b), (d) spin polarization were extracted from the corresponding data sets in Figs. 1(d)–1(g). Black lines correspond to fits to the data (see text for details). The data were obtained at  $h\nu = 6$  eV at a temperature of ~130 K.

energy contour and  $\phi_k = 0$  corresponds to the positive  $k_x$  axis. By contrast, for p polarization, we find roughly a  $\sin^2 \phi_k$  behavior, while, additionally, a significant intensity asymmetry for  $k_x \to -k_x$  is observed. This asymmetry is commonly termed linear dichroism and can be attributed to the light electric field that breaks  $k_x \to -k_x$  symmetry in p-polarized geometry [Fig. 1(a)] [37].

Next, we compare the photoelectron intensity distributions to the corresponding spin distributions. Using s-polarized light, the measured  $S_y$  component of the photoelectron spin polarization displays a nearly ideal  $(-\cos\phi_k)$  dependence [Figs. 1(f) and 2(b)]. Similar to the intensity, changing to p-polarized light also modifies the  $S_y$  momentum distribution. First, we observe roughly a  $(\cos\phi_k)$  dependence for  $S_y$ , indicating an overall sign reversal between s and p polarization in accordance with previous work [12,14,15,18]. Furthermore, the broken  $k_x \to -k_x$  symmetry manifests in the  $S_y$  distribution, showing that linear dichroism not only affects the intensity, but also the photoelectron spin polarization.

The main experimental observations, including large photoelectron spin polarizations, are captured by the results of our one-step photoemission theory in Figs. 1(h) and 1(i). In particular, the calculations confirm the observed sign reversal of  $S_v$  between s- and p-polarized light. The TSS is derived from p orbitals, while the photoelectron final state  $\Phi_f$  at hv = 6 eV is predominantly s-like in the present case [16,38]. Within the dipole approximation, this yields selection rules for the matrix element  $\langle \Phi_f | \mathbf{E} \cdot \mathbf{r} | \Psi_{TSS} \rangle$ . In particular, for this simplified form of  $\Phi_f$ , the electric field components  $\mathcal{E}_{x,y,z}$  of the light electric vector **E** couple exclusively to the correspondingly aligned  $p_{x,y,z}$  orbitals of the TSS [13,14]. Exploiting this orbital selectivity, we adopt a simple model that captures the main features observed in the experimental data. To first order, the wave function of the TSS can be represented as  $|\Psi_{TSS}\rangle = \gamma |p_z, \uparrow_{\phi}\rangle - i\beta |p_r|$  $\uparrow_{\phi}\rangle + \alpha |p_t, \downarrow_{\phi}\rangle$  [7]. Here,  $|p_r\rangle = \cos \phi_k |p_x\rangle + \sin \phi_k |p_y\rangle$  and  $|p_t\rangle = -\sin\phi_k|p_x\rangle + \cos\phi_k|p_y\rangle$  are radial and tangential orbital textures, and  $|\uparrow_{\phi}(\downarrow_{\phi})\rangle = (1/\sqrt{2})[+(-)ie^{-i\phi_k}|\uparrow_z\rangle +$  $|\downarrow_z\rangle$  stand for left-handed and right-handed helical spin textures.

For s polarization, the light electric field  $\mathbf{E} = (0, \mathcal{E}_{v}, 0)$ couples predominantly to the  $p_v$  orbital contribution. The above model predicts a term  $\delta I_s \sim \Delta \cos^2 \phi_k$  that modulates the momentum distribution of the photoelectron intensity along the Fermi surface. The parameter  $\Delta = \alpha^2 - \beta^2$  reflects the imbalance between radial  $p_r$  and tangential  $p_t$  contributions to  $\Psi_{TSS}$  or, equivalently, the  $\phi_k$ -dependent weight of  $p_v$ orbitals. The form of  $\delta I_s$  is in good agreement with the experimental data, as seen in Fig. 2(a). We find  $\Delta > 0$  implying a predominantly tangential character of the in-plane orbitals, in agreement with findings for Bi<sub>2</sub>Se<sub>3</sub> [13]. The amplitude of the modulation  $\delta I_s$  amounts to ca. 10% of the total intensity. The sign and also the absolute value of  $\Delta$  thus compare reasonably well with the  $p_r$  and  $p_t$  contributions to the TSS obtained previously in density functional theory (DFT) calculations for Bi<sub>2</sub>Se<sub>3</sub> [7,13]. Accordingly, the measured momentum distribution of  $S_{\nu}$  is expected to reflect the  $p_{\nu}$ -projected spin texture of  $\Psi_{TSS}$ . For the y component of the  $p_y$ -projected spin texture, one obtains  $P_{y} \sim -\cos\phi_{k}$  [7], which indeed closely matches the experimental data in Fig. 2(b).

For p polarization, the light electric field  $\mathbf{E} = (\mathcal{E}_x, 0, \mathcal{E}_z)$  couples to  $p_x$  and  $p_z$  orbitals. We find that the azimuthal modulation of the intensity involves two terms, namely,  $\delta I_{p1} \sim \Delta \sin^2 \phi_k$  and  $\delta I_{p2} \sim \alpha \gamma \cos \phi_k$ . The first term  $\delta I_{p1}$  is analogous to  $\delta I_s$ . It originates from the  $\mathcal{E}_x$  component of the light field and reflects the  $\phi_k$  dependence of the  $p_x$  orbital weight in  $\Psi_{TSS}$ . The second term  $\delta I_{p2}$  describes the intensity asymmetry between  $+k_x$  and  $-k_x$ , i.e., the above-mentioned linear dichroism. Within our simplified model, this term scales with the parameters  $\alpha$  and  $\gamma$ , and thus originates from the mixing of  $p_x$  and  $p_z$  orbitals. Our data indicate that indeed both terms contribute appreciably to the total intensity. A superposition of  $\delta I_{p1}$  and  $\delta I_{p2}$  nicely reproduces the  $\phi_k$  dependence of the measured intensity distribution [Fig. 2(c)].

The behavior of the photoelectron spin polarization  $S_v$  likewise becomes more complex for p than for s polarization. First, one gets terms reflecting the y components of the  $p_z$ and  $p_x$ -projected spin textures of the TSS, which in both cases leads to  $S_{v1} \sim \cos \phi_k$  [7]. This leading term already is in rather good agreement with the experimental data in Fig. 2(d). Yet, there is another term  $S_{y2}$  which is of similar origin as the linear dichroism  $\delta I_{p2}$  in the intensity distribution. To illustrate this, we consider  $\Psi_{TSS}$  at  $\phi_k = \frac{\pi}{2}$ , where the relevant  $p_z p_x$ -projected contribution to  $\Psi_{TSS}$  can be written as  $|\uparrow_{v}\rangle(\gamma|p_{z}\rangle - i\alpha|p_{x}\rangle) + |\downarrow_{v}\rangle(\gamma|p_{z}\rangle + i\alpha|p_{x}\rangle)$ , for a spin quantization chosen along y. The difference of  $\pi$  in the phase between the  $p_z$  and  $p_x$  orbitals for  $|\uparrow_y\rangle$  and  $|\downarrow_y\rangle$  will, in general, yield an intensity difference between the  $|\uparrow_{v}\rangle$  and  $|\downarrow_y\rangle$  photoelectrons of  $I_{\uparrow} - I_{\downarrow} \sim \alpha \gamma \operatorname{Im}(T_z^* T_x)$ , with the matrix elements  $T_z \sim \langle \Phi_f | E_z z | p_z \rangle$  and  $T_x \sim \langle \Phi_f | E_x x | p_x \rangle$ . As a result, there is a finite photoelectron spin polarization  $S_{v2}$ at  $\phi_k = \frac{\pi}{2}$ , although the orbital-projected spin polarizations of  $\Psi_{TSS}$  along y vanish. This spin polarization  $S_{y2}$  is indeed observed experimentally, as seen in Figs. 1(g) and 1(d). The measured azimuthal dependence is reasonably well captured by the sum of the leading term  $S_{v1}$  and  $S_{v2} \sim \sin^2 \phi_k$ . The term  $S_{y2}$  reflects the mixing of  $p_x$  and  $p_z$  orbitals in  $\Psi_{TSS}$ and the fact that unlike the y components, the x components of the  $p_x$ - and  $p_z$ -projected spin textures have different  $\phi_k$ dependences [7].

The above analysis shows how the measured spin and intensity momentum distributions qualitatively reflect the orbital texture and the orbital-dependent spin texture of the TSS across full momentum space. Up to now, we focused on the situation where the behavior of the TSS is, in good approximation, isotropic and the influence of the  $C_{3v}$  symmetry of the crystal lattice is negligible. Next we will discuss measurements for  $\mathrm{Bi}_2\mathrm{Te}_3(0001)$  for which the in-plane potential with  $C_{3v}$  symmetry gives rise to an appreciable hexagonal warping of the TSS dispersion. The in-plane potential is expected to induce an out-of-plane component  $P_z$  in the spin texture of the TSS [39–41]. According to DFT calculations and symmetry considerations [39,41],  $P_z$  shows a threefold azimuthal modulation, becomes maximal along  $\bar{\Gamma}\bar{K}$ , and vanishes in the mirror planes, i.e., along  $\bar{\Gamma}\bar{M}$ .

Figure 3 shows spin-resolved ARPES measurements for Bi<sub>2</sub>Te<sub>3</sub>(0001) focusing on the z component of the photoelectron spin polarization  $S_z$ . As seen in Fig. 3(a), the Fermi surface of the TSS acquires a snowflake shape with cusps along  $\bar{\Gamma}\bar{M}$  [41,42]. To study  $S_z$  in dependence of the

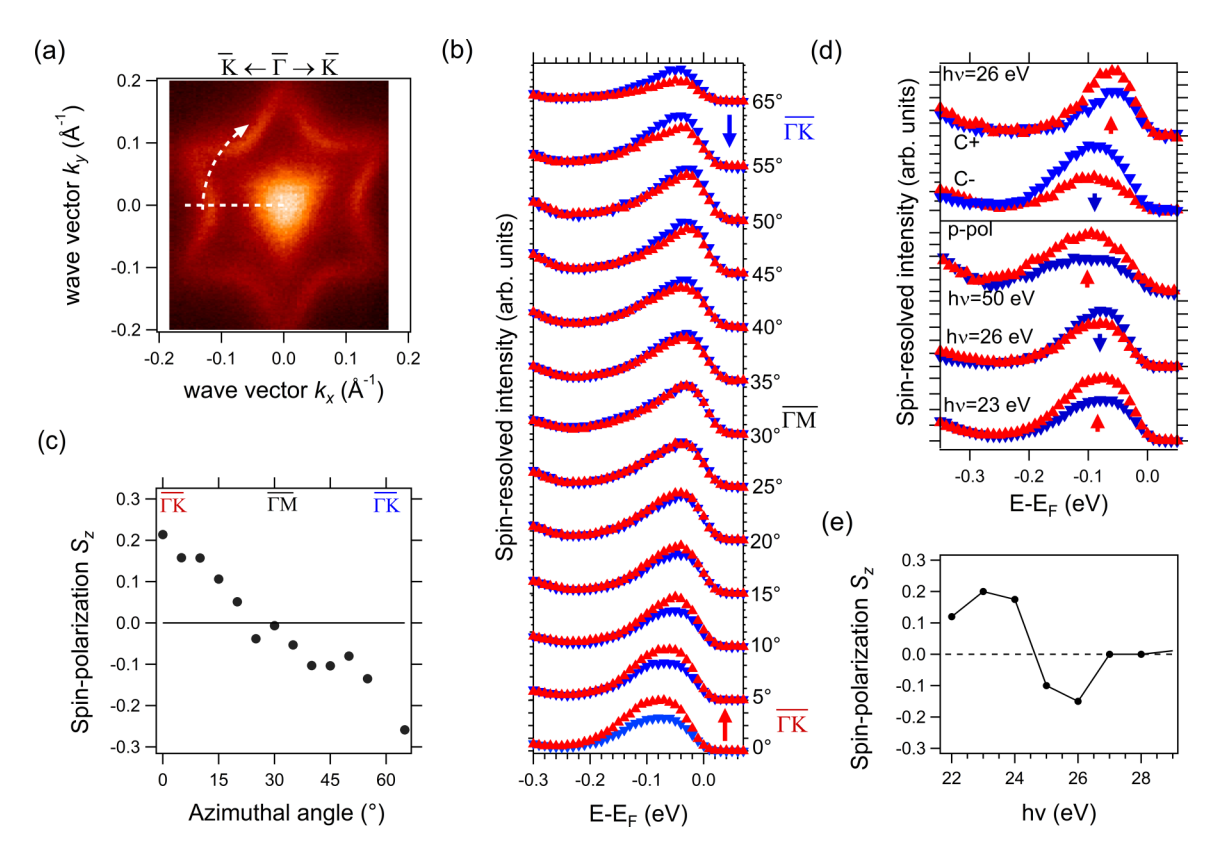


FIG. 3. (a) ARPES data set of the Fermi surface in Bi<sub>2</sub>Te<sub>3</sub>(0001) ( $h\nu=23$  eV). The outer, snowflake-shaped feature arises from the topological surface state. The arrow indicates the azimuthal rotation of the sample performed to obtain the data in (b). (b) Spin-resolved energy distribution curves (EDCs) measured along different crystalline directions, as summarized in (c). The EDCs were taken at an emission angle of 3° corresponding to approximately  $k_{||}=0.12~\text{Å}^{-1}$  at the Fermi level. The spin-quantization axis is along z. The EDCs were measured at wave vectors in the plane of light incidence, while the crystalline orientation was varied by azimuthal sample rotation. (d) Spin-resolved EDCs for an orientation along  $\bar{\Gamma}\bar{K}$  measured at different  $h\nu$  for p polarization and for circularly left and right polarized light. (e) Photon-energy dependence of the measured  $S_z$  for p-polarized light. All measurements were carried out at a temperature of  $\sim$ 70 K.

azimuthal angle, we consider spin-resolved energy distribution curves (EDCs) in Fig. 3(b). The EDCs were measured at wave vectors  $k_x$  within the plane of light incidence, while the crystalline orientation was varied by rotating the sample along the azimuthal direction. The measured  $S_z$  nicely reproduces the  $\phi_k$ -dependent characteristics expected for an in-plane potential with  $C_{3v}$  symmetry, as discussed above [Figs. 3(b) and 3(c)]. Nevertheless, we find that the physical origin of the measured  $S_z$  is not immediately the intrinsic spin texture. This becomes clear by considering the data in Figs. 3(d) and 3(e), where for the same crystalline orientation along  $\bar{\Gamma}\bar{K}$ , the measured  $S_z$  varies and even changes sign with both photon energy and polarization.

To understand the effect, we may model the wave function of the TSS along  $k_x$  as  $|\Psi_{TSS}\rangle = [|p_{xz}\rangle + \cos(3\varphi_k)|\delta p_y\rangle]|\uparrow_y\rangle + [|p_y\rangle + \cos(3\varphi_k)|\delta p_{xz}\rangle]|\downarrow_y\rangle$ , where  $\delta p_y$  and  $\delta p_{xz}$  are orbital admixtures to the respective spinor components introduced by the  $C_{3v}$  symmetry. Coefficients are omitted for clarity. Here,  $\varphi_k$  describes the azimuthal crystalline orientation relative to the  $k_x$  axis and  $\varphi_k = 0$  corresponds to the  $\bar{\Gamma}\bar{K}$  direction. For the fully isotropic case, the admixtures vanish and  $\Psi_{TSS}$  reduces to the form discussed above, where the spinor components are strictly even and odd functions. The spin polarization of the TSS along

z is then given by  $P_z \sim \cos(3\varphi_k) \operatorname{Re}[\langle \delta p_y | p_y \rangle \langle p_{xz} | \delta p_{xz} \rangle]$ , i.e., it scales with the orbital admixtures introduced by the in-plane potential. On the other hand, for the photoelectron spin polarization for p-polarized light, one finds  $S_z \sim \cos(3\varphi_k) \operatorname{Re}[\langle \Phi_f | \mathbf{E} \cdot \mathbf{r} | \delta p_{xz} \rangle \langle p_{xz} | \mathbf{E} \cdot \mathbf{r} | \Phi_f \rangle]$ . For both  $P_z$  and  $S_z$ , the  $\cos(3\varphi_k)$  periodicity reflects the azimuthal modulation of  $\Psi_{TSS}$ . Yet, the magnitude and also the sign of  $S_z$  is determined by the transition matrix elements which depend on the final state  $\Phi_f$ . The latter is the origin of the experimentally observed  $h\nu$  dependence of  $S_z$ . In the case of circularly polarized light, the expression for  $S_z$  is further modified and also contains matrix elements involving  $p_y$  orbitals, which manifests in the observed polarization dependence.

Our one-step photoemission calculations for Bi<sub>2</sub>Te<sub>3</sub>(0001) qualitatively confirm a  $h\nu$  dependence of  $S_z$ . In Fig. 4, we present calculated ARPES data sets where the red/blue color code refers to the photoelectron spin polarization  $S_z$ . One can see that  $S_z$  reverses between the two considered photon energies and further shows a dependence on the wave vector, as seen for the sign change along negative  $k_{||}$  in Fig. 4(a). The latter effect can be attributed to a  $k_{||}$ -dependent orbital composition of the TSS, but goes beyond the present experimental data obtained at fixed  $k_{||}$ .

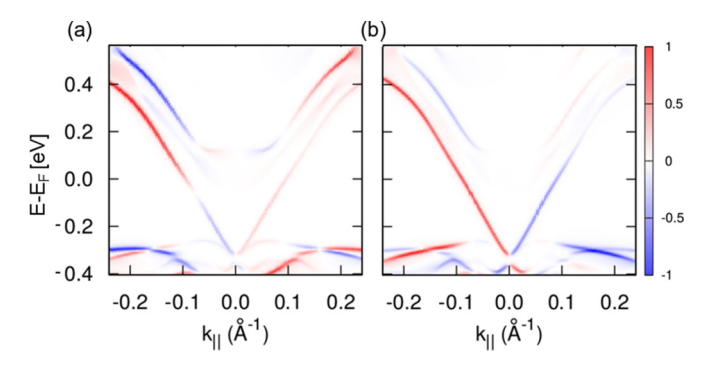


FIG. 4. One-step photoemission calculations for Bi<sub>2</sub>Te<sub>3</sub>(0001) of the angle-resolved photoelectron spin polarization  $S_z$  along  $\bar{\Gamma}\bar{K}$  for p-polarized light with (a)  $h\nu=24$  eV and (b)  $h\nu=38$  eV. The wave vector  $k_{\parallel}$  lies in the plane of light incidence.

In summary, we studied the photoelectron intensity and spin distributions in 2D momentum space for the topological surface state in Bi<sub>2</sub>(Te,Se)<sub>3</sub>(0001). Supported by one-step photoemission theory and model considerations, the data unveil the full momentum dependence of the coupled spin and orbital textures of the surface state. As these textures are related directly to the topological electronic

properties, our findings will be particularly relevant for the study of novel topological materials with complex Fermi surfaces [43–46], and may even enable the investigation of spin-dependent Berry-curvature signatures in these systems [47].

We acknowledge financial support from the DFG through Grant No. RE1469/13-1, SFB 1170 (projects A01 and B01) and the Würzburg-Dresden Cluster of Excellence on Complexity and Topology in Quantum Matter-ct.qmat (EXC 2147, Project No. 390858490). Part of the ARPES measurements was performed with the approval of the Proposal Assessing Committee of the Hiroshima Synchrotron Radiation Center (Proposals No. 15-A-36 and No. 15-A-75). J.M. would like to thank the CEDAMNF (Grant No. CZ.02.1.01/0.0/0.0/15\_-003/0000358) co-funded by the ERDF as part of the Ministry of Education, Youth and Sports of Czech Republic. J.B. and H.E. acknowledge financial support by the DFG via Projects No. Eb 158/32 and No. Eb 158/36. We gratefully acknowledge the financial support of the EU ERC-AG Program (Project No. 3-TOP). O.E.T. and K.A.K. acknowledge support from the Russian Science Foundation (Grant No. 17-12-01047), and ISP SB RAS and IGM SB RAS state assignment.

- [1] M. König, S. Wiedmann, C. Brüne, A. Roth, H. Buhmann, L. W. Molenkamp, X. Qi, and S. Zhang, Science 318, 766 (2007).
- [2] M. Z. Hasan and C. L. Kane, Rev. Mod. Phys. 82, 3045 (2010).
- [3] P. Dziawa, B. J. Kowalski, K. Dybko, R. Buczko, A. Szczerbakow, M. Szot, E. Łusakowska, T. Balasubramanian, B. M. Wojek, M. H. Berntsen *et al.*, Nat. Mater. 11, 1023 (2012).
- [4] C.-Z. Chang, J. Zhang, X. Feng, J. Shen, Z. Zhang, M. Guo, K. Li, Y. Ou, P. Wei, L.-L. Wang et al., Science 340, 167 (2013).
- [5] N. P. Armitage, E. J. Mele, and A. Vishwanath, Rev. Mod. Phys. 90, 015001 (2018).
- [6] M. M. Otrokov, I. I. Klimovskikh, H. Bentmann, D. Estyunin, A. Zeugner, Z. S. Aliev, S. Gaß, A. U. B. Wolter, A. V. Koroleva, A. M. Shikin *et al.*, Nature (London) **576**, 416 (2019).
- [7] H. Zhang, C.-X. Liu, and S.-C. Zhang, Phys. Rev. Lett. 111, 066801 (2013).
- [8] Z.-H. Zhu, C. N. Veenstra, G. Levy, A. Ubaldini, P. Syers, N. P. Butch, J. Paglione, M. W. Haverkort, I. S. Elfimov, and A. Damascelli, Phys. Rev. Lett. 110, 216401 (2013).
- [9] D. Hsieh, Y. Xia, L. Wray, D. Qian, A. Pal, J. H. Dil, J. Osterwalder, F. Meier, G. Bihlmayer, C. L. Kane *et al.*, Science 323, 919 (2009).
- [10] M. S. Bahramy, P. D. C. King, A. de la Torre, J. Chang, M. Shi, L. Patthey, G. Balakrishnan, P. Hofmann, R. Arita, N. Nagaosa et al., Nat. Commun. 3, 1159 (2012).
- [11] S. R. Park, J. Han, C. Kim, Y. Y. Koh, C. Kim, H. Lee, H. J. Choi, J. H. Han, K. D. Lee, N. J. Hur *et al.*, Phys. Rev. Lett. 108, 046805 (2012).
- [12] C. Jozwiak, C.-H. Park, K. Gotlieb, C. Hwang, D.-H. Lee, S. G. Louie, J. D. Denlinger, C. R. Rotundu, R. J. Birgeneau, Z. Hussain *et al.*, Nat. Phys. 9, 293 (2013).

- [13] Y. Cao, J. A. Waugh, X.-W. Zhang, J.-W. Luo, Q. Wang, T. J. Reber, S. K. Mo, Z. Xu, A. Yang, J. Schneeloch *et al.*, Nat. Phys. 9, 499 (2013).
- [14] Z.-H. Zhu, C. N. Veenstra, S. Zhdanovich, M. P. Schneider, T. Okuda, K. Miyamoto, S.-Y. Zhu, H. Namatame, M. Taniguchi, M. W. Haverkort, I. S. Elfimov, and A. Damascelli, Phys. Rev. Lett. 112, 076802 (2014).
- [15] Z. Xie, S. He, C. Chen, Y. Feng, H. Yi, A. Liang, L. Zhao, D. Mou, J. He, Y. Peng *et al.*, Nat. Commun. 5, 3382 (2014).
- [16] J. Sanchez-Barriga, A. Varykhalov, J. Braun, S.-Y. Xu, N. Alidoust, O. Kornilov, J. Minár, K. Hummer, G. Springholz, G. Bauer *et al.*, Phys. Rev. X 4, 011046 (2014).
- [17] C. Seibel, J. Braun, H. Maaß, H. Bentmann, J. Minár, T. V. Kuznetsova, K. A. Kokh, O. E. Tereshchenko, T. Okuda, H. Ebert et al., Phys. Rev. B 93, 245150 (2016).
- [18] H. L. Meyerheim and C. Tusche, Phys. Status Solidi (RRL) Rapid Res. Lett. **12**, 1870337 (2018).
- [19] J. H. Dil, Electron. Struct. 1, 023001 (2019).
- [20] C. Tusche, M. Ellguth, A. Krasyuk, A. Winkelmann, D. Kutnyakhov, P. Lushchyk, K. Medjanik, G. Schönhense, and J. Kirschner, Ultramicroscopy 130, 70 (2013).
- [21] C. Tusche, A. Krasyuk, and J. Kirschner, Ultramicroscopy 159, 520 (2015).
- [22] C. Jozwiak, J. A. Sobota, K. Gotlieb, A. F. Kemper, C. R. Rotundu, R. J. Birgeneau, Z. Hussain, D.-H. Lee, Z.-X. Shen, and A. Lanzara, Nat. Commun. 7, 13143 (2016).
- [23] D. Vasilyev, C. Tusche, F. Giebels, H. Gollisch, R. Feder, and J. Kirschner, J. Electron. Spectrosc. Relat. Phenom. 199, 10 (2015).
- [24] H. Maaß, S. Schreyeck, S. Schatz, S. Fiedler, C. Seibel, P. Lutz, G. Karczewski, H. Bentmann, C. Gould, K. Brunner *et al.*, J. Appl. Phys. **116**, 193708 (2014).

- [25] S. Schreyeck, K. Brunner, A. Kirchner, U. Bass, S. Grauer, C. Schumacher, C. Gould, G. Karczewski, J. Geurts, and L. W. Molenkamp, J. Phys.: Condens. Matter 28, 145002 (2016).
- [26] T. Okuda, K. Miyamaoto, H. Miyahara, K. Kuroda, A. Kimura, H. Namatame, and M. Taniguchi, Rev. Sci. Instrum. 82, 103302 (2011).
- [27] T. Okuda, K. Miyamoto, A. Kimura, H. Namatame, and M. Taniguchi, J. Electron Spectrosc. Relat. Phenom. 201, 23 (2015).
- [28] K. A. Kokh, S. V. Makarenko, V. A. Golyashov, O. A. Shegai, and O. E. Tereshchenko, Cryst. Eng. Commun. 16, 581 (2013).
- [29] H. Ebert, D. Ködderitzsch, and J. Minár, Rep. Prog. Phys. 74, 096501 (2011).
- [30] J. Braun, J. Minár, and H. Ebert, Phys. Rep. 740, 1 (2018).
- [31] See Supplemental Material at http://link.aps.org/supplemental/ 10.1103/PhysRevB.103.L161107 for additional details describing the theoretical photoemission calculations.
- [32] S. V. Halilov, H. Gollisch, E. Tamura, and R. Feder, J. Phys.: Condens. Matter 5, 4711 (1993).
- [33] M. Potthoff, J. Lachnitt, W. Nolting, and J. Braun, Phys. Status Solidi (b) 203, 441 (1997).
- [34] R. Feder, J. Phys. C 14, 2049 (1981).
- [35] J. Braun, Rep. Prog. Phys. 59, 1267 (1996).
- [36] G. Malmström and J. Rundgren, Comput. Phys. Commun. 19, 263 (1980).

- [37] H. Bentmann, H. Maaß, E. E. Krasovskii, T. R. F. Peixoto, C. Seibel, M. Leandersson, T. Balasubramanian, and F. Reinert, Phys. Rev. Lett. 119, 106401 (2017).
- [38] J. H. Ryoo and C.-H. Park, Phys. Rev. B 93, 085419 (2016).
- [39] L. Fu, Phys. Rev. Lett. 103, 266801 (2009).
- [40] S. Souma, K. Kosaka, T. Sato, M. Komatsu, A. Takayama, T. Takahashi, M. Kriener, K. Segawa, and Y. Ando, Phys. Rev. Lett. 106, 216803 (2011).
- [41] J. Henk, A. Ernst, S. V. Eremeev, E. V. Chulkov, I. V. Maznichenko, and I. Mertig, Phys. Rev. Lett. 108, 206801 (2012).
- [42] Y. L. Chen, J. G. Analytis, J.-H. Chu, Z. K. Liu, S.-K. Mo, X. L. Qi, H. J. Zhang, D. H. Lu, X. Dai, Z. Fang *et al.*, Science 325, 178 (2009).
- [43] I. Zeljkovic, Y. Okada, C.-Y. Huang, R. Sankar, D. Walkup, W. Zhou, M. Serbyn, F. Chou, W.-F. Tsai, H. Lin *et al.*, Nat. Phys. 10, 572 (2014).
- [44] F. Reis, G. Li, L. Dudy, M. Bauernfeind, S. Glass, W. Hanke, R. Thomale, J. Schäfer, and R. Claessen, Science 357, 287 (2017).
- [45] C.-H. Min, H. Bentmann, J. N. Neu, P. Eck, S. Moser, T. Figgemeier, M. Ünzelmann, K. Kissner, P. Lutz, R. J. Koch et al., Phys. Rev. Lett. 122, 116402 (2019).
- [46] N. B. M. Schröter, S. Stolz, K. Manna, F. D. Juan, M. G. Vergniory, J. A. Krieger, D. Pei, T. Schmitt, P. Dudin, T. K. Kim et al., Science 369, 179 (2020).
- [47] M. Schüler, U. D. Giovannini, H. Hübener, A. Rubio, M. A. Sentef, and P. Werner, Sci. Adv. 6, eaay2730 (2020).